SEPTEMBER 13 2018

Analytical coupled vibro-acoustic modeling of a cavity-backed duct-membrane system with uniform mean flow

Yang Liu; Jingtao Du; Li Cheng

J. Acoust. Soc. Am. 144, 1368–1380 (2018)
https://doi.org/10.1121/1.5053586

Analytical coupled vibro-acoustic modeling of a cavity-backed duct-membrane system with uniform mean flow

Yang Liu,[1] Jingtao Du,[1,a)] and Li Cheng[2]
[1]*College of Power and Energy Engineering, Harbin Engineering University, Harbin, 150001, China*
[2]*Department of Mechanical Engineering, The Hong Kong Polytechnic University, Hong Kong, 999077, China*

(Received 10 June 2018; revised 17 August 2018; accepted 21 August 2018; published online 13 September 2018)

Sound propagation in a flow duct is a complex and technically challenging problem. The presence of flexible vibrating walls inside the duct creates additional difficulties to the problem due to the complex vibro-acoustic and aero-acoustic couplings involved in the system. An accurate prediction of the coupled system response is of great importance for a good understanding of the underlying physics as well as the optimal design of relevant noise suppression devices. In the present work, a unified energy formulation is proposed for the fully coupled structural-acoustic modelling of a duct-mounted membrane backed by an acoustic cavity with a grazing flow. Sufficiently smoothed admissible functions, taking the form of a combination of Fourier series and supplementary polynomials, are constructed to overcome the differential discontinuities for various boundary and/or coupling conditions. The formulation allows the obtention of all relevant vibro-acoustic field information in conjunction with the generalized Lighthill equation and Rayleigh-Ritz procedure. The validation and convergence studies show the accuracy and the efficiency of the proposed model. Results show the strong structural-acoustic interaction in such a duct-membrane-cavity system, and the flow affects resonant amplitude of membrane-dominant modes significantly. Some cross-zones can be observed for the membrane kinetic energy frequency response with low Mach number cases, especially when a higher tension is applied to the membrane. Analyses on the structural-acoustic coupling strength indicate that the coupling between the odd-even structural modes becomes more significant at a higher Mach number compared with odd-odd and even-even mode pairs. It is also shown that adjusting the boundary constraint of the membrane or imposing a higher tensile force allows impairing the adverse influence of the flow in the duct on sound attenuation. https://doi.org/10.1121/1.5053586

[NX] Pages: 1368–1380

I. INTRODUCTION

Vibro-acoustic coupling problems have been extensively studied for several decades, exemplified by the classical problem of the sound radiation from a vibrating structure into an enclosed space. Analytical solutions can be derived for simple configurations using methods such as modal coupling theory, acoustic Green's function method, or energy principle.[1–3] Owing to the physical features and the flexibility of the analytical modelling, studies on elementary configurations shed light on the important underlying physics governing the structural-acoustic coupling phenomena. Generally speaking, resonant frequencies of the coupled system differ from the *in vacuo* structural modes and those of the cavity with rigid walls, as a result of the vibro-acoustic interaction between the two sub-systems. In more practical situations such as air-conditioning and ventilation systems, in which a flexible structure is mounted in a hard-walled duct, and the sound radiation from the structure into the duct is coupled with the sound waves propagating from the upstream of the duct, forming another typical type of interaction between the flexible structure and a confined sound space. In this case, full solutions for the acoustic pressure spectral density have been obtained by Doak.[4] Considering a square duct with a non-rigid sidewall, the coupling between the acoustic propagation in the duct and the structural vibration of the duct wall was studied by Cabelli,[5,6] with results showing that a large number of acoustic modes should be taken into account in order to achieve an accurate prediction of the coupling near the system resonance or at high frequencies. Subsequently, with the proposed concept of the acoustic "break-out" and "break-in" through duct walls by Cummings and Astley,[7–9] a fully coupled structure-duct-cavity model has attracted much attention. Subsequently, significant progress was made in various aspects such as sound transmission, radiation to the exterior, and structural/acoustic coupling analyses. Characterized by the sound transmission loss between the upstream and downstream sound waves in a duct, a fully coupled modelling is of great importance for duct silencer design. From this perspective, a series of work has been carried out by Huang,[10] and his subsequent theoretical and experimental studies show that such a silencer can provide satisfactory sound attenuations in the low-to-medium frequency range over roughly one octave band, when properly designed.

In applications such as heating, ventilating, and air-conditioning duct systems, it is essential to consider the effect of the grazing flow, thus giving rise to additional aero-

a)Electronic mail: dujingtao@hrbeu.edu.cn

acoustic coupling. The sound propagation in a flow duct is more complex in the presence of the flow when considering the flow-induced vibration or turbulence. The classical approach uses Green's functions, expressed as a linear combination of acoustic modes. The approach has been used to solve the radiation of a vibration source inside a duct with uniform mean flow.[11,12] The coupled response of a duct-plate-cavity system in the presence of a subsonic uniform mean flow was obtained by Bodony[13] using Green's functions combined with the Galerkin method. Using the same method, Zhang *et al.*[14] carried out theoretical investigations on a so-called drum-like silencer with mean flow, with focus put on the thermo-acoustic instability. Meanwhile, other numerical studies and experiments were also conducted to investigate the influence of the flow. For example, Choy *et al.*[15] experimentally investigated the flow-induced vibration of a two-dimensional membrane covering part of the duct walls. Their studies show that negligible vibration was induced by the flow when the tension applied to the membrane was either too low or too high. FEMLAB was utilized by Choy and Huang[16] to compute the solution of the partial differential equations on a duct-membrane-cavity coupling system. A time-domain numerical approach in a uniform flow duct was presented by Fan *et al.*,[17] which allowed some details of the panel structural responses and the transmission loss to be captured. Using the fourth order Runge-Kutta procedure, a vortex propagating across a drum-like silencer conveying a mean flow was also studied by Tang and coworkers.[18,19] Although several methods have been proposed for the vibro-acoustic study of such complex duct-structural-acoustic coupling systems with mean flow, most of them are based on purely numerical/experimental approaches or modelled via analytical means with some sort of limitation, such as structural boundary conditions. The influence of various important system parameters as well as the coupling mechanism are not well understood, which hinders the optimal design and implementation of such a vibro-acoustic coupling system.

Motivated by this, an analytical coupled vibro-acoustic analysis model of a cavity-backed duct-membrane system with uniform mean flow is proposed in this paper. The proposed model aims at providing an alternative tool to the existing numerical and experimental approaches for the study of such complex structural-acoustical interaction systems. A unified energy formulation, inspired by our previous studies[20,21] in combination with the generalized Lighthill equation and Rayleigh-Ritz procedure, is proposed. Compared with other modeling approaches, the proposed method can account for the flow and entire vibro-acoustic coupling process of the duct-membrane-cavity system in an efficient way leading to the following benefits: (i) the model is built up using the sub-system Lagrangian. Its modular nature thus facilitates the inclusion of various additional dynamic/acoustic components or devices into the proposed general framework; (ii) the model considers more general structural boundaries while allowing flexible analysis on the coupling mechanism.

The paper is organized as follows. Details of the formulation are given in Sec. II. Results and discussions are shown in Sec. III. First, the reliability and the convergence of the proposed approach are verified. Based on the model established, structural-acoustic response of the membrane is addressed in detail. Then the duct-membrane coupling as well as cavity-membrane coupling are investigated to reveal the coupling mechanisms with mean flow. Influences of the boundary restraining stiffness and those of the tensile force on sound attenuation at various flow velocities are analyzed. Finally, conclusions are drawn.

II. FORMULATION AND SOLUTION METHODOLOGY

A. Problem description

A two-dimensional (2-D) fully coupled system is considered. The system consists of a duct, a backing-cavity, and a flexible structure (a tensioned membrane by default) with arbitrary boundary conditions, as shown in Fig. 1. Relevant parameters are also illustrated, i.e., structure length L, duct height h, and cavity depth h_c, respectively. The membrane is subjected to harmonic planar acoustic waves at grazing incidence in the presence of a uniform mean flow with a low Mach number in the duct. In the current study, a low flow velocity and a high-tension force are adopted to avoid the flow-induced flexural instability. The incident harmonic plane acoustic wave is defined as $P_i = \dot{P}_i e^{-ik_0^+ x + i\omega t}$, where $\dot{P}_i$ is the amplitude of the pressure wave and ω is angular frequency. $k_0^+ = \omega/[c_0(1+M_a)]$ is the acoustic wave number, with $M_a = U/c_0$ being the Mach number of the uniform axial flow in the duct, in which c_0 and U are the sound speed and flow velocity in the duct, respectively. S_1 and S_2 denote the transverse spring stiffness coefficients to simulate arbitrary boundary conditions.

B. Energy formulation of the duct-membrane coupling system

An analytical solution for the entire duct-membrane-cavity system is presented in this section. An equivalent and convenient way for tackling this problem is the energy formulation, the solution of which will be sufficiently accurate if a proper set of smooth admissible functions can be constructed in the entire physical domain of the system including the boundary and various coupling interfaces. In addition, the energy formulation offers the potential benefits

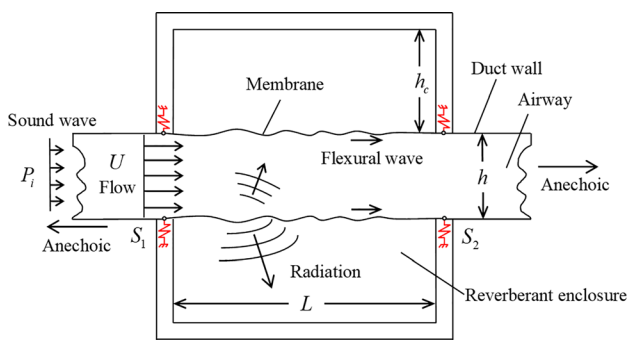

FIG. 1. (Color online) Schematic of the coupled duct-membrane-cavity system in the presence of mean flow.

of being extended to treat more complex duct configurations with multiple subsystems.

The system Lagrangian includes the total potential energy, the total kinetic energy, and the work done by various sound pressure components P_i, P_{rad}, or P_{cav}. Here, P_i is the sound pressure propagating from upstream of the duct, P_{rad} is the radiated sound pressure due to the membrane vibration, and P_{cav} is the sound pressure of the lower surface coupled with the backing-cavity. One yields

$$L_{memb} = U_{memb}^{potential} - T_{memb}^{kinetic} + \vartheta_{P_i}^{work} + \vartheta_{P_{rad}}^{work} - \vartheta_{P_{cav}|_{y=0}}^{work}, \tag{1}$$

$$L_{cav} = U_{cav}^{potential} - T_{cav}^{potential} + \vartheta_{V_{lower}}^{work}, \tag{2}$$

where $\vartheta_{P_{cav}|_{y=0}}^{work}$ denotes the work done by the sound pressure P_{cav} of the backing-cavity acting on the membrane and $\vartheta_{V_{lower}}^{work}$ denotes the work on the acoustic cavity due to the lower membrane surface vibration. The continuity conditions on the membrane-fluid interface implies a reciprocity relationship, that is, $\vartheta_{P_{cav}|_{y=0}}^{work} = \vartheta_{V_{lower}}^{work}$. Equations (1) and (2) can be further written as

$$L_{memb} = \frac{1}{2}\int_0^L F\left(\frac{\partial u}{\partial x}\right)^2 dx + f(S_1, S_2, u) - \frac{1}{2}\int_0^L m_s\left(\frac{\partial u}{\partial t}\right)^2 dx + \int_0^L u(P_{rad} + P_i - P_{cav})dx, \tag{3}$$

$$L_{cav} = \frac{1}{2\rho_0 c_0^2}\int_s P_{cav}^2 ds - \frac{1}{2\rho_0\omega^2}\int_s \left[\left(\frac{\partial P_{cav}}{\partial x}\right)^2 + \left(\frac{\partial P_{cav}}{\partial y}\right)^2\right] ds + \int_0^L u P_{cav} dx, \tag{4}$$

where u is the transverse displacement of the membrane, F and m_s are, respectively, the tensile force applied on the flexible membrane and its mass per unit area, and $f(S_1, S_2, u)$ is the boundary potential energy stored in the elastic springs S_1 and S_2, as shown in Fig. 1. This yields

$$f(S_1, S_2, u) = \left[S_1 u^2(0) + S_2 u^2(L)\right]/2. \tag{5}$$

Obviously, the interaction among the duct, membrane and cavity is reflected in the work items $\vartheta_{P_{rad}}^{work}$ and $\vartheta_{V_{lower}}^{work}$, which will become much complex for the description of such a structural-acoustic interaction in the presence of mean flow.

Once the energy description of the duct-membrane system is formulated, the remaining task is to construct the appropriate admissible function, and then all the unknown coefficients can be found using the Rayleigh-Ritz procedure. For the classical fixed boundary condition, the transverse displacement of vibrating string is usually expanded as the Fourier series, namely,

$$u(x) = \sum_{n=0}^{\infty} a_n \cos\lambda_n x. \tag{6}$$

For the vibrating membrane, in contrast to the beam or rod, the structural flexibility associated with the transverse vibration is generated by the tensing force applied at its both ends. This is also reflected in the boundary equilibrium equations for the elastic restraint, namely,

$$F\frac{\partial u(x,t)}{\partial x}\Big|_{x=0} = S_1 u(0,t) \quad \text{at } x = 0, \tag{7}$$

$$F\frac{\partial u(x,t)}{\partial x}\Big|_{x=L} = S_2 u(L,t) \quad \text{at } x = L. \tag{8}$$

It can be seen that the direct use of the standard Fourier series Eq. (6) in the elastic boundary conditions, Eqs. (7) and (8), generates a boundary discontinuity, which will significantly deteriorate the solution convergence and accuracy. In order to overcome this problem, the following improved decomposition series is constructed for the string flexural displacement:

$$u(x) = \sum_{n=0}^{\infty} a_n \cos\lambda_n x + b_1\zeta_1(x) + b_2\zeta_2(x),$$
$$\zeta_1(x) = x\left(\frac{x}{L} - 1\right)^2, \quad \zeta_2(x) = \frac{x^2}{L}\left(\frac{x}{L} - 1\right), \tag{9}$$

where $\lambda_n = n\pi/L$ and $\zeta_1(x)$ and $\zeta_2(x)$ are two supplementary functions, with b_1 and b_2 being the corresponding weight coefficients. It is easy to observe that

$$\zeta_1(0) = \zeta_1(L) = \zeta'_1(L) = 0, \quad \zeta'_1(0) = 1, \tag{10}$$

$$\zeta_2(0) = \zeta_2(L) = \zeta'_2(0) = 0, \quad \zeta'_2(L) = 1. \tag{11}$$

Using the above series, the boundary differential discontinuities associated with the traditional Fourier series can be removed, and the base function set is now sufficiently smooth in the entire solving interval from 0 to L including both end points. Similarly, to ensure the inherent continuity over the structural-acoustic interface, the sound pressure inside the acoustical cavity can be accordingly expanded as

$$p_{cav} = \sum_{m_x=0}^{\infty}\sum_{m_y=0}^{\infty} A_{m_x m_y}\cos\lambda_{m_x}x\cos\lambda_{m_y}y + \frac{y^2}{h_c}\left(\frac{y}{h_c} - 1\right)\sum_{n=0}^{\infty} q_n\cos\lambda_n x. \tag{12}$$

The purpose of adding the polynomial term can be understood from the relationship between the sound pressure and the particle vibrational velocity, namely, $\partial p/\partial n = -j\omega\rho_0 u_n$. It can be observed that the original double Fourier series expansion will encounter the differential discontinuity on the structural-acoustic coupling interface. The introduction of auxiliary terms will alleviate the differential jump, thus improving the accuracy and convergence of series solution.

C. Duct acoustics with mean flow

The flexible membrane mounted in a rectangular duct can be seen as a distributed acoustic source, and the spectral density of the acoustic pressure in the duct with non-

reflecting terminations under no-flow conditions has been derived by Doak.[4] Similarly, the aerodynamic sound generation can also be considered as a linear superposition of the propagating modes, except that both the positive and negative z-direction propagating waves radiated by the flexible membrane are affected by the presence of the uniform flow, which makes the analytical treatment more complex than the case in stationary media. Also, the appearance of a discontinuity in the normal particle velocity near the upper side of the membrane as the kinematic effect of the shear layer should be considered. In practical cases, the stream-wise velocity of the fluid in the thin layer near the membrane surface decreases due to viscous effect of the flow. Meanwhile, there is also a large velocity gradient along the direction normal to the membrane surface inside the shear layer. In the current model, with the assumption of ignoring the viscosity in fluid, the shear layer reduces to an infinitely thin sheet which separates a region without flow (membrane surface) and an acoustic field in the flow.[23] The normal particle velocities in the two sides of the layer are different due to the presence of the fluid. In our model, the procedure presented by Ingard[24] is followed to deal with this discontinuity in the normal particle velocity as

$$V^d = (\partial u/\partial t + U\partial u/\partial x) = (V + U/i\omega\partial V/\partial x), \tag{13}$$

where V^d and V are the particle velocities near the flow and over the membrane surface, respectively, both being normal to the membrane surface. A unified fundamental equation governing the generation of sound in the presence of both uniform flow and solid boundaries derived by Goldstein[22] is written

$$P_{rad}(x,t) = \frac{1}{c_0^2}\int_{-T}^{T}\int_0^L \rho_0 V^d \frac{D_0 G(x',\tau|x,t)}{D\tau}dx'd\tau, \tag{14}$$

where

$$\frac{D_0}{D\tau} = \frac{\partial}{\partial\tau} + U\frac{\partial}{\partial x}, \tag{15}$$

with ρ_0 being the air mass density and G the Green's function for a point source in a hard-walled duct with uniform mean flow, which has been extensively studied.[11,12] So, the radiated sound pressure from the vibrating membrane in duct is given by

$$P_{rad}(x,y) = \frac{\rho_0}{2h}\sum_{m=0}^{\infty}\frac{\omega - Uk_m^{\pm}}{\alpha_m k_0^+}(2-\delta_{0m})\cos\left(\frac{m\pi}{h}y\right)\int_0^L V^d \times \Re\left(k_m^{\pm}\right)dx', \tag{16}$$

where δ_{0m} represents the Kronecker delta function; k_m^+ and k_m^- correspond to the positive and negative z-direction propagating waves, respectively; and m is the transverse duct mode index. Specific expressions of these quantities are written as

$$k_m^{\pm} = \left(\frac{\pm\alpha_m - M_a}{1-M_a^2}\right),\quad \alpha_m = \sqrt{1-\frac{\kappa_m^2}{\left(k_0^+\right)^2}(1-M^2)},$$
$$\kappa_m^2 = \frac{m^2\pi^2}{h^2}, \tag{17}$$

in which the integrand $V^d \times \Re(k_m^{\pm})dx'$ in Eq. (16) represents a point mass source, the integral sum of the acoustic fields due to the point source distribution gives the overall radiated acoustic pressure into the duct. The expression of $\Re(k_m^{\pm})$ is given by

$$\Re(k_m^{\pm}) = H(x-x')e^{-ik_m^+(x-x')} + H(x'-x)e^{-ik_m^-(x-x')}, \tag{18}$$

where H is the Heaviside function. Equation (18) shows that, by setting the observing point x at the center of the membrane, the integral in Eq. (16) can be split into two parts, corresponding to the positive and negative x-direction propagating waves due to the two parts of membrane vibration $\{(0-x)$ and $(x-L)\}$. For x-coordinates located beyond the downstream edge of membrane, Eq. (16) can be simplified as

$$P_{rad}(x,y) = \frac{\rho_0}{2h}\sum_{m=0}^{\infty}\frac{\omega - Uk_m^+}{\alpha_m k_0^+}(2-\delta_{0m})\cos\left(\frac{m\pi}{h}y\right)\int_0^L V^d \times e^{-ik_m^+(x-x')}dx'. \tag{19}$$

Furthermore, when the excitation frequency is much lower than the cut-on frequency of the duct, the radiated sound wave that propagates into the far-field downstream the duct will be just the zero-order wave ($m=0$). Therefore, the radiated sound field in the downstream far-field can be written as

$$P_{rad}(x,y)|_{x\to+\infty} = \frac{\rho_0}{2h}\sum_{m=0}^{\infty}\frac{\omega - Uk_0^+}{\alpha_m k_0^+}e^{-ik_0^+x}\int_0^L V^d \times e^{ik_0^+x'}dx'. \tag{20}$$

D. Solution of the vibro-acoustic coupled response

By substituting the constructed admissible functions [Eq. (9)] and the radiated sound pressure [Eq. (16)] into the coupled system Lagrangian [Eq. (1)] and getting the derivative with respect to the unknown coefficients $a_{n'}$, a set of linear equations can then be obtained, namely,

$$\sum_{n=0}^{\infty}(K_{nn'} - \omega^2 M_{nn'} + C_{nn'}^{rad})a_n - \sum_{m_x=0}^{\infty}\sum_{m_y=0}^{\infty}C_{m_x m_y n'}^{cav}A_{m_x m_y} = C_{n'}^i, \tag{21}$$

where $K_{nn'}$ and $M_{nn'}$ are the stiffness and mass terms of the *in vacuo* elastically restrained membrane, respectively, given by

$$K_{nn'} = \frac{L}{2}F\lambda_n\lambda_{n'}\delta_{nn'} + S_1 + S_2(-1)^{n+n'},$$
$$M_{nn'} = Lm_s\delta_{nn'}\frac{1+\delta_{0n'}}{2}. \tag{22}$$

Using Eq. (16) yields

$$C_{nn'}^{rad} = \frac{\rho_0}{2h}\sum_{m=0}^{\infty}\frac{\omega - Uk_m^{\pm}}{\alpha_m k_0^{+}}(2-\delta_{0m})\cos\left(\frac{m\pi}{h}y\right) \times \int_0^L \cos\lambda_{n'}x \int_0^L \left(\cos\lambda_n x' + \frac{\lambda_n iU}{\omega}\sin\lambda_n x'\right) \times \Re\left(k_m^{\pm}, x', x\right)dx'dx. \tag{23}$$

The derivatives corresponding to $a_{n'}$ in the work done by the sound pressure P_{cav} in the backing-cavity are given by

$$C_{m_x m_y n'}^{cav} = \cos\lambda_{m_y} y|_{y=h_c}\int_0^L \cos\lambda_n x\cos\lambda_{m_x}x dx = (-1)^{m_y}\frac{L}{2}\delta_{m_x n'}\frac{1+\delta_{0n'}}{2}. \tag{24}$$

The derivatives of the work done by harmonic forcing pressure are written

$$C_{n'}^{i} = \frac{ik_0^{+}L^2(1-e^{-ik_0^{+}L}\cos n'\pi)}{\left(n'^2\pi^2 - \left(k_0^{+}\right)^2L^2\right)}. \tag{25}$$

Second, substituting the membrane displacement and the cavity sound pressure function into Eq. (12), the derivative with respect to the unknown coefficients $A_{m'_x m'_y}$ in Eq. (12) is solved and linear system equations in terms of $A_{m_x m_y}$ is obtained as

$$\sum_{m'_x}^{\infty}\sum_{m'_y}^{\infty}(K_{m_x m_y, m'_x m'_y}^{cav} - \omega^2 M_{m_x m_y, m'_x m'_y}^{cav})A_{m_x m_y} + \sum_{n=0}^{\infty} C_{m_x m_y n'}^{cav} a_n = 0, \tag{26}$$

in which the stiffness and mass terms for the cavity subsystem can be expressed, respectively, as

$$K_{m_x m_y, m'_x m'_y}^{cav} = \frac{Lh_c}{2\rho_0\omega^2}\left[\lambda_{m_x}\lambda_{m'_x}\delta_{m_x m'_x}\delta_{m_y m'_y}\frac{1+\delta_{0m_y}}{2} + \lambda_{m_y}\lambda_{m'_y}\delta_{m_y m'_y}\delta_{m_x m'_x}\frac{1+\delta_{0m_x}}{2}\right], \tag{27}$$

$$M_{m_x m_y, m'_x m'_y}^{cav} = \frac{Lh_c}{2}\frac{1}{\rho_{air}c_0^2} \times \left[\lambda_{m_x}\lambda_{m'_x}\delta_{m_x m'_x}\delta_{m_y m'_y}\frac{1+\delta_{0m_x}}{2}\frac{1+\delta_{0m_y}}{2}\right]. \tag{28}$$

Similarly, the unknown coefficients b_1, b_2, and q_n in Eqs. (9) and (12) can be processed in the same way. For the sake of briefness, corresponding linear system of equations about b_1, b_2, and q_n are not given here.

The above linear equations given in Eqs. (21) and (26) can be rewritten in a matrix form, respectively, as

$$(\mathbf{K} - \omega^2\mathbf{M} + i\omega\mathbf{C_{rad}})\mathbf{A} - \mathbf{C_{cav}}\mathbf{B} = -\mathbf{C_i}, \tag{29}$$

$$\left(\mathbf{M_{cav}} - \frac{\mathbf{K_{cav}}}{\omega^2}\right)\mathbf{B} + \mathbf{C_{cav}^T}\mathbf{A} = 0, \tag{30}$$

where $\mathbf{A}$ and $\mathbf{B}$ are the vectors that contain all the unknown Fourier expansion coefficients including $a_0,\ldots, a_n$, b_1, b_2 and $A_{00},\ldots,A_{m_x m_y}$, $q_0,\ldots,q_n$, respectively. Elements in other matrices presented in above equations correspond to the terms shown in Eqs. (21) and (26). Solving the simultaneous equations yields

$$(\mathbf{K} - \omega^2\mathbf{M} + i\omega\mathbf{C_{rad}})\mathbf{A} + \mathbf{C_{cav}}\left(\mathbf{M_{cav}} - \frac{\mathbf{K_{cav}}}{\omega^2}\right)^{-1}\mathbf{C_{cav}^T}\mathbf{A} = -\mathbf{C_i}. \tag{31}$$

By truncating the infinite Fourier series to a finite number of terms, $m_x = m_y = M_{cavity}$, $n = n' = N$, $m = M_{duct}$, a system of linear equations of finite size with $a_0,\ldots,a_n$, b_1, b_2 and $A_{00},\ldots,A_{m_x m_y}$, $q_0,\ldots,q_n$ as unknowns are obtained. With the expansion coefficients solved, the transverse vibration displacement at any point across the membrane, and the sound pressure inside both the cavity and the duct can be directly obtained from Eqs. (9), (12), and (16).

III. RESULTS AND DISCUSSIONS

A. Verification and convergence analysis

For verifications, a benchmark problem investigated by Choy[16] is revisited. The model consists of a double cavity-backed fixed flexible membrane in an infinite duct in the presence of a uniform mean flow. The present simulations use the same set of model parameters as the reference paper,[16]

$$h_c = h = 0.1\,\text{m}, \quad L = 5h, \quad c_0 = 340\,\text{m/s},$$
$$\rho_0 = 1.255\,\text{kg/m}^3, \quad F^* = \frac{F}{\rho_0 c_0^2 h} = 0.54,$$
$$m_s^* = \frac{m_s}{\rho_0 h} = 1.3,$$

where m_s^* is the mass ratio and F^* is the dimensionless tensile force.

The fixed boundary condition for the membrane is simulated by setting the elastic spring stiffness, $S_1 = S_2 = 1 \times 10^9$ N/m. To guarantee the calculation convergence and accuracy in a wide frequency region, the wave modes up to $M_{duct} = 40$ are employed to calculate the sound radiation from the membrane into the duct. Meanwhile, the improved Fourier series expansion terms for membrane vibration and cavity sound pressure are truncated up to $N = 20$ and $M_{cavity} = 15$, respectively, for which accurate enough results can be derived as previously studied.[21] The validation is conducted through comparisons with the numerical solutions for Ma = 0.03 and 0.045, respectively (see Ref. 16 for details), in which the measurement results are also given to further verify the current model experimentally, as shown in Fig. 2. It can be seen that both sets of results agree well, thus demonstrating the correctness of the proposed model. The

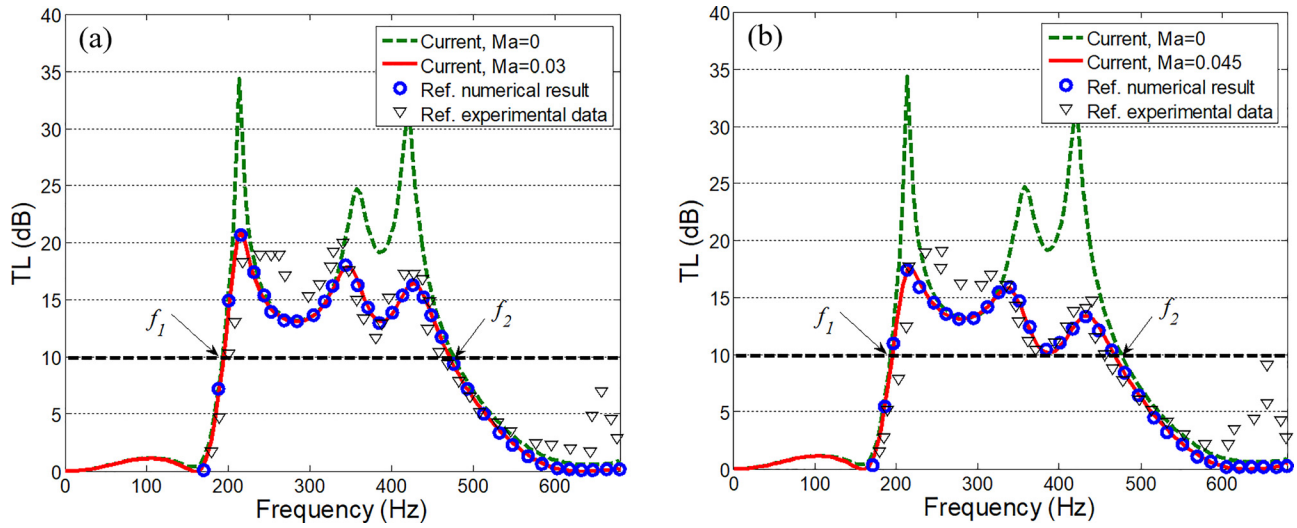

FIG. 2. (Color online) Comparison among the numerical result, experimental data and current calculations with different Mach numbers (a) Ma = 0.03, (b) Ma = 0.045.

reference result is obtained using FEMLAB®, which is based on the finite element method. Slight differences between the two sets of results, albeit noticeable at certain frequencies in Fig. 2, are deemed as acceptable. This is mainly due to the inherent differences between these two approaches. The presence of flow causes a significant decrease in the transmission loss, especially near the resonant frequencies. With the increase of the mean flow Mach number, further decreasing trend of transmission loss can be observed.

In Eqs. (9) and (12), the admissible functions constructed by the improved Fourier series expansion are used to guarantee sufficiently smooth property in the whole solving domain including the boundary and/or coupling interface. Actually, the introduction of the supplementary polynomials into the standard Fourier series will improve and guarantee the convergence and the accuracy. In order to demonstrate the rapid convergence of the present approach, the Galerkin method combined with Green's function for the cavity pressure calculation is also presented here for comparisons. To search for the optimal truncated terms N' for the membrane vibration based on the level of amplitude of the Fourier coefficients in Eq. (9), the truncated numbers M_{duct} and M_{cvity} are kept the same as aforementioned. The normalized root mean square velocity of the membrane, $V_{rms} = (\sum_n |i\omega a_n|^2/N')^{1/2}$, is used as the reference value and the ratio of $V_{rms}/|i\omega a_n| > 10^{1.5}$ is chosen as the evaluation index to obtain the appropriate truncated terms N', which is actually pre-defined, and also verified in the subsequent numerical calculation. Figure 3(a) shows the optimal truncated terms N' with respect to the excitation frequency and Mach number. Overall, as the Mach number or frequency increases, more items are needed to achieve the preset evaluation index. Figure 3(b) shows the amplitude distribution of each $|a_n|$ at 526.3 Hz with four different flow velocities corresponding to Fig. 3(a), with the x-z view being plotted in Fig. 3(c). Obviously, eight terms seem to be sufficient in the present case as shown in Fig. 3(a).

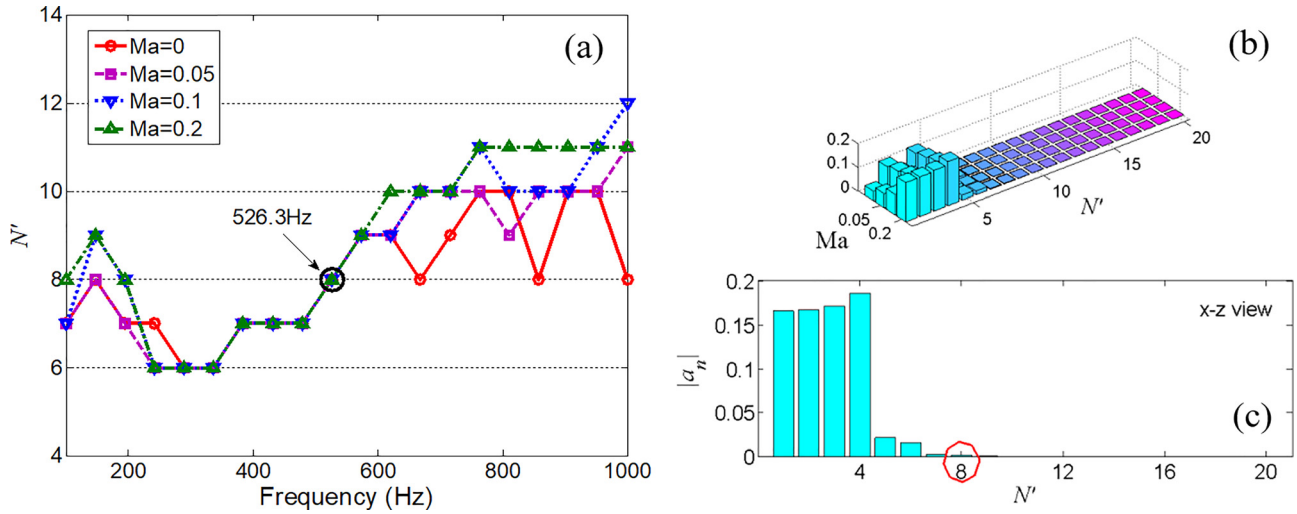

FIG. 3. (Color online) The convergence characteristic analysis for the current method: (a) The optimal truncated number N'; (b) variation of $|a_n|$ with Ma; (c) the x-z view of (b).

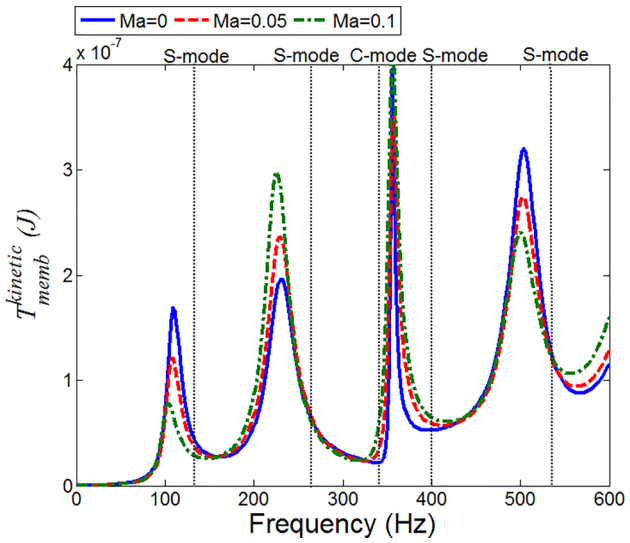

FIG. 4. (Color online) Total kinetic energy of membrane with different Mach numbers at $F^* = 0.2$.

Compared with another analytical method,[10] for which the Green's function is utilized to describe the sound pressure in a cavity radiated by a vibrating wall, a solution needs to be obtained in each frequency step. For the current energy formulation, however, the major calculation components used in Eqs. (29) and (30), such as $\mathbf{M}_{\mathbf{cav}}$, $\mathbf{K}_{\mathbf{cav}}$, and $\mathbf{C}_{\mathbf{cav}}$, can be pre-calculated for each sub-system, and used as the standard sub-modules in subsequent frequency response simulation, which contributes to enhance the calculation efficiency.

B. Vibro-acoustic response behavior

In this section, the dynamic response of the membrane under the plane wave excitation and mean flow effect are calculated to investigate the vibro-acoustic behavior in such a system. To quantify the membrane vibration response, the total kinetic energy $T^{\text{kinetic}}_{\text{memb}}$ of the membrane is presented in Fig. 4 with different low Mach numbers ($\text{Ma} = 0.05$ and $\text{Ma} = 0.1$). The material and geometrical parameters are the same as those used in Fig. 2, except for the dimensionless tensile force ($F^* = 0.2$ is used here).

The vertical dashed lines correspond to the modal frequencies of the membrane *in vacuo* and those of the cavity with rigid walls, denoted by S-mode and C-mode, respectively. Strong coupling in the duct-cavity-membrane system can be clearly seen from the significant shift of the coupled resonance peaks as compared with the uncoupled counterparts. With the increase of Mach numbers, vibration response amplitudes of the membrane at resonance are greatly affected, while the peak frequencies are relatively stable at such low Mach numbers. For the higher tension membrane at low Mach numbers, the mass and stiffness matrices dominate the membrane vibration, which is why there is little frequency shift for higher tension plates. However, the flow changes the pressure field source strength as given in Eq. (16), then the vibration amplitudes at resonance are significantly affected.

The total kinetic energies $T^{\text{kinetic}}_{\text{memb}}$ corresponding to an increased tensile force of $F^* = 0.5$ are also calculated and presented in Fig. 5(a). The figure shows three cross-zones marked by circles, in which $T^{\text{kinetic}}_{\text{memb}}$ undergoes very slight (or even invisible) changes for the three low Mach numbers used in the simulation. Meanwhile, a fluctuating trend in $T^{\text{kinetic}}_{\text{memb}}$ level can be found as the mean flow speed increases, and the whole spectrum can be separated into four regions by these three cross-zones. Variations of frequencies corresponding to each cross-zone with the tension force are plotted in Fig. 5(b). Obviously, frequencies around the first and third cross-zones are increased with F^*, which means that they are dominated by the membrane modes. The red dashed lines with a circle represent the frequency of the second cross-zone under various cavity depths $L = 4.5h_c$, $5h_c$, and $5.5h_c$. The natural frequencies of the hard-walled cavity are also given in the figure by blue solid circles, namely, 307, 340, and 378 Hz. It can be found that the second cross-zone closely corresponds to the cavity mode and is almost unaffected by the membrane tension.

Vibration velocity distributions $|V|$ across the membrane are presented in Fig. 6(a) at $f = 331$ Hz around the second cross-zone. Although the kinetic energy is unaffected by the mean flow in the cross-zone, $|V|$ fluctuates, albeit little. Plotted in Fig. 6(b) is the corresponding sound pressure distribution in the duct. It can be seen that despite the slight

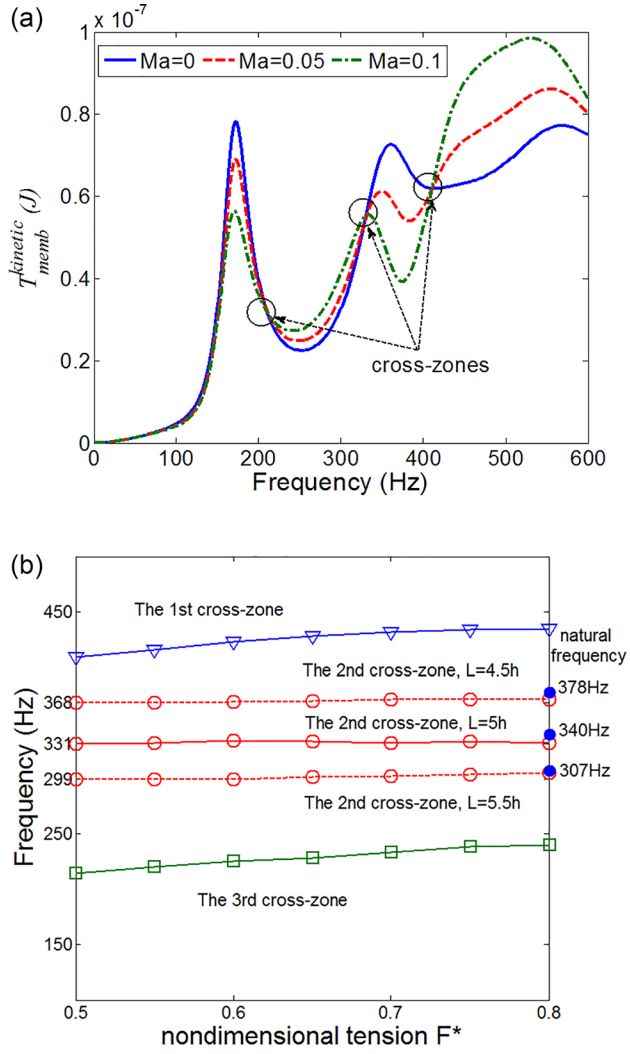

FIG. 5. (Color online) (a) Total kinetic energy of membrane for different Mach numbers at $F^* = 0.5$, (b) cross-zone frequencies under different tension F^*.

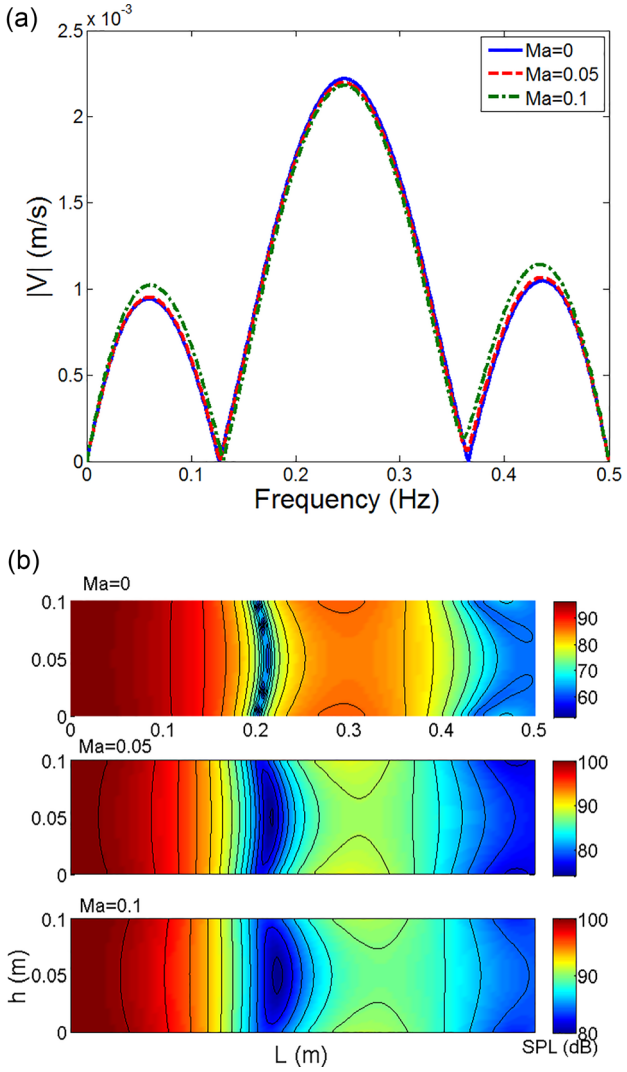

FIG. 6. (Color online) Vibro-acoustic response distributions for the coupling system at the excitation frequency of 331 Hz under $F^* = 0.5$. (a) Membrane velocity distribution, (b) sound pressure field in duct.

differences in $|V|$, a significant difference in its distribution pattern can be observed. This phenomenon can be understood in that sound radiation into duct is affected by the presence of flow through the dependence of duct acoustic mode on Mach number as shown in Eq. (16). Moreover, the flow has the effect of modifying the pressure field source strength through the term proportional to $U\partial V/\partial x$ in Eq. (13).

C. Coupling analysis

To analyze the vibro-acoustic coupling characteristics in the system, the coupling coefficients will be formulated to evaluate the coupling strength, and to investigate the flow effect on the structural-acoustic interaction mechanism. Further expanding the supplementary functions into Fourier series, one will get

$$u(x) = \sum_{q=1}^{Q}\left[u_q\varphi_q(x)\right] = \sum_{q=1}^{Q}\left[\left(\sum_{n=0}^{\infty} a_{nq} + b_{1q} + b_{2q}\right)\varphi_q(x)\right], \tag{32}$$

where u_q is the modal amplitude and a_{nq}, b_{1q}, and b_{2q} are the Fourier expansion coefficients. For the fixed membrane, modal basis function can be expressed as $\varphi_q(x) = \sin(q\pi x/L)$.

Combining Eq. (32) and $V_q/i\omega = u_q$, the system matrix equation shown in Eq. (31) can be rewritten as

$$\sum_{q'=1}^{N}\left(i\omega\{\mathbf{M}\}_{q,q'} + \frac{\{\mathbf{K}\}_{q,q'}}{i\omega} + \{\mathbf{C_{rad}}\}_{q,q'} + \left\{\mathbf{C_{cav}}\left(\mathbf{M_{cav}} - \frac{\mathbf{K_{cav}}}{\omega^2}\right)^{-1}\mathbf{C_{cav}^T}/i\omega\right\}_{q,q'}\right)V_{q'} = -\{\mathbf{C_i}\}_q, \tag{33}$$

which can be expressed in terms of modal amplitude as

$$V_q\frac{i\omega L m_s}{2} + \{\alpha_{qq}\}_{s\text{-}s}V_q + \sum_{q'}\{\alpha_{qq'}\}_{s\text{-}d}V_{q'} + \sum_{q'}\{\alpha_{qq'}\}_{s\text{-}c}V_{q'} = -\{\mathbf{C_i}\}_q, \tag{34}$$

in which $\{\alpha_{qq'}\}_{s\text{-}s}$ represents the inter-modal structural-structural (s-s) coupling coefficients between mode q' and mode q. Thanks to the orthogonality of the modal functions, it can be proven that the even-odd modal coupling coefficients are equal to zero. Similarly, $\{\alpha_{qq'}\}_{s\text{-}d}$ represents the structural-acoustic (duct) coupling coefficient. Finally, $\{\alpha_{qq'}\}_{s\text{-}c}$ is the structural-acoustic (cavity) coupling coefficient, which is independent of the mean flow.

In the subsequent study, an evaluation index for the coupling strength, defined as $\gamma_{qq'} = \log_{10}\{\alpha_{qq'}\}_{s\text{-}d}/\{\alpha_{qq}\}_{s\text{-}s}$, is used to quantify the coupling strength between different mode pairs. The influence of the Mach number and the excitation frequency are studied separately. Variations of $\gamma_{qq'}$ with the flow velocity are plotted at 200 and 600 Hz in Figs. 7(a) and 7(b), respectively. Obviously, the coupling strengths for higher-order modes are weak, being roughly one or a few orders of magnitude lower than γ_{11}. The structural-acoustic coupling strengths for the odd-odd and even-even mode pairs are insensitive to the mean flow, especially at low flow velocities. On the contrary, the odd-even modes are more strongly coupled at higher Mach numbers. Alongside the increase of the flow velocity, the coupling strengths for these modes gradually increase as a general trend. Effect of the excitation frequency on the coupling strength is also illustrated in Fig. 8, showing a gradual increase for different Mach numbers.

In order to get a whole picture of the influence of the mean flow and excitation frequency, the contour plots of $\gamma_{qq'} = \log_{10}\{\alpha_{qq'}\}_{s\text{-}d}/\{\alpha_{qq}\}_{s\text{-}s}$ at different Mach numbers are shown in Fig. 9. Comparing γ_{11} and γ_{13} shown in Figs. 9(a) and 9(b), some weak coupling regions ($\gamma < 0$ marked in grey) start to appear when the mode order increases, and the gradients in these two maps vary slowly with the increase of the mean flow effect. When $\gamma_{qq'} = 0$, the structural-acoustic coupling is of the same level as that of the self-structural coupling. For the odd-even modes plotted in Figs. 9(c) and 9(d), more weak coupling regions are found, and the value

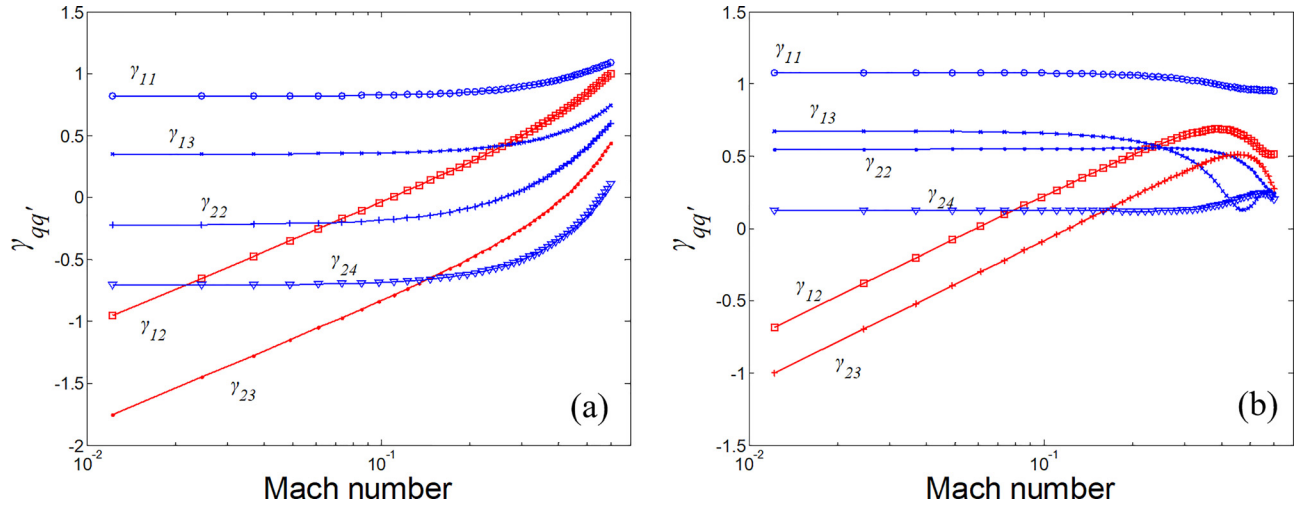

FIG. 7. (Color online) Coupling strength $\gamma_{qq'}$ variation with Mach number for different excitation frequencies (a) $f_{exc} = 200$ Hz, (b) $f_{exc} = 600$ Hz.

of γ is generally smaller than the odd-odd mode pairs, especially for the low Mach numbers. Moreover, a significant gradient for the coupling strength can be observed, in which the variation of γ by more than one order of magnitude is marked with the circles in Fig. 9(c). For the even-even modes, as shown in Figs. 9(e) and 9(f), the variation trend of the coupling strength is similar with those of their odd-odd counterparts. In general, it can be found that the coupling strength will be gradually decreased with the increase of mode order.

The coupling strength between the membrane and the cavity, quantified by $\gamma'_{qq'} = \log_{10}\{\alpha_{qq'}\}_{s\text{-}c}/\{\alpha_{qq}\}_{s\text{-}s}$, is also studied. $\gamma'_{qq'}$ varies with the frequency, as shown in Fig. 10. Corresponding contours for the odd-odd and even-even mode pairs are presented in Figs. 10(a) and 10(b), respectively. Two resonant peaks can be observed in this figure, namely, 340 and 680 Hz, corresponding to the first and second modes of the backing cavity, respectively. The dashed line with circles in the figure corresponds to a negative infinity (logarithmic scale), indicating the decoupling between any odd (even) and even (odd) mode pair. Since the coupling coefficient $\{\alpha_{qq'}\}_{s\text{-}c}$ is related to the interaction matrix for cavity and membrane $\mathbf{C_{cav}}$, as shown in Eqs. (29) and (30), the above phenomenon can be explained through the definition of $\mathbf{C_{cav}}$, namely,

$$C^{cav}_{m_y qq'} = \cos\lambda_{m_y} y|_{y=h_c} \int_0^L \sin\lambda_{q'} x \cos\lambda_{q-1} x dx = \begin{cases} (-1)^{m_y} \dfrac{nL}{\pi} \dfrac{(-1)^{q+q'-1} - 1}{(q-1)^2 - (q')^2}, & q - 1 \neq q', \\ 0, & q - 1 = q'. \end{cases} \tag{35}$$

Obviously, when $q + q' - 1$ is even, the interaction terms (q, q') in $\mathbf{C_{cav}}$ are zero. Through matrix operation shown in Eq. (33), one can find that the coefficients $\{\alpha_{odd\text{-}even}\}_{s\text{-}c}$ are also zeros.

D. Sound attenuation performance

System parameters such as the boundary restraining stiffness and tensile force applied to the membrane could be tuned to achieve a desired silencing performance. This issue

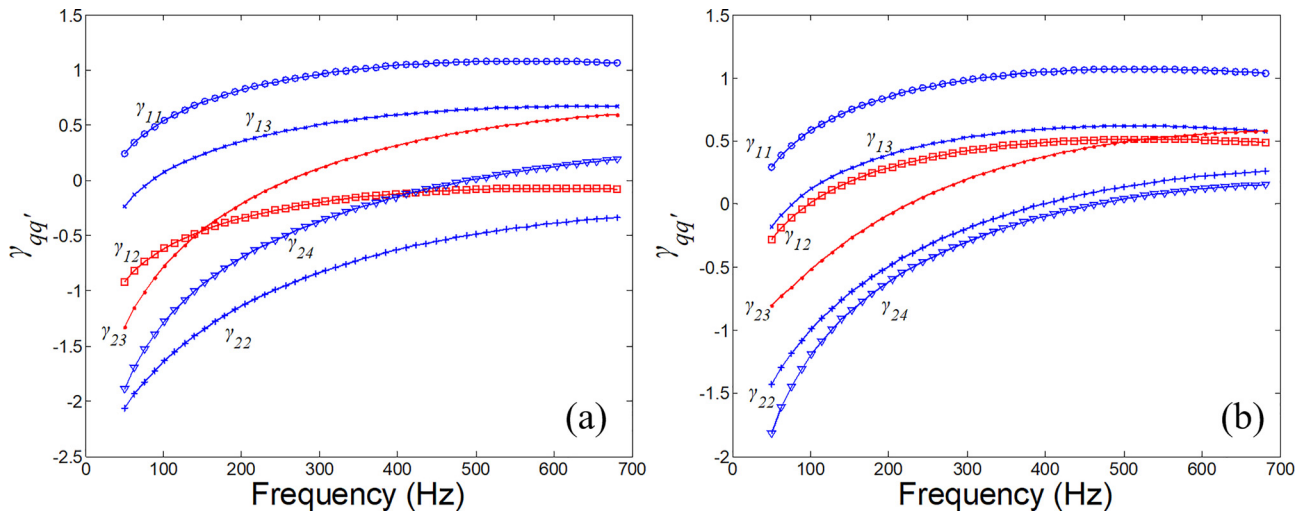

FIG. 8. (Color online) Coupling strength $\gamma_{qq'}$ variation with excitation frequency for different Mach number (a) Ma = 0.05, (b) Ma = 0.2.

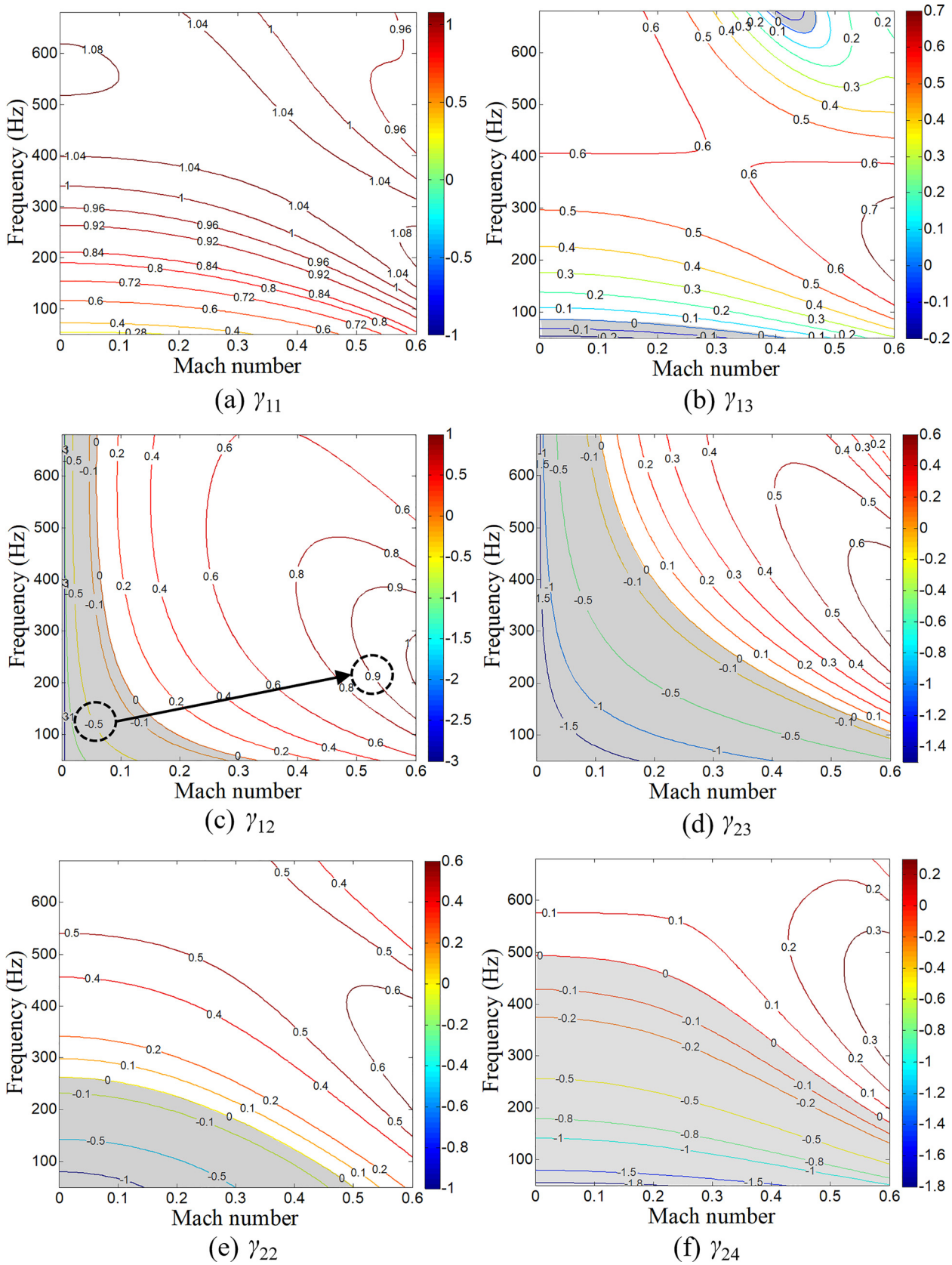

FIG. 9. (Color online) Coupling strength $\gamma_{qq'}$ as functions of Mach number and excitation frequency.

is explored in the presence of uniform mean flow. System parameters are set as $h_c = h = 0.17$ m, $L = 2.5h$, and $m_s = \rho_0 h$. A so-called sound attenuation band $[f_1, f_2]$ is determined as the frequency range in which a minimum of 10 dB TL is obtained, as shown in Fig. 2. The ratio f_2/f_1 is the objective function to be maximized. Figure 11 illustrates the distribution pattern of f_2/f_1 as a function of the boundary spring stiffness S_1 and S_2 with the Ma number taken as 0,

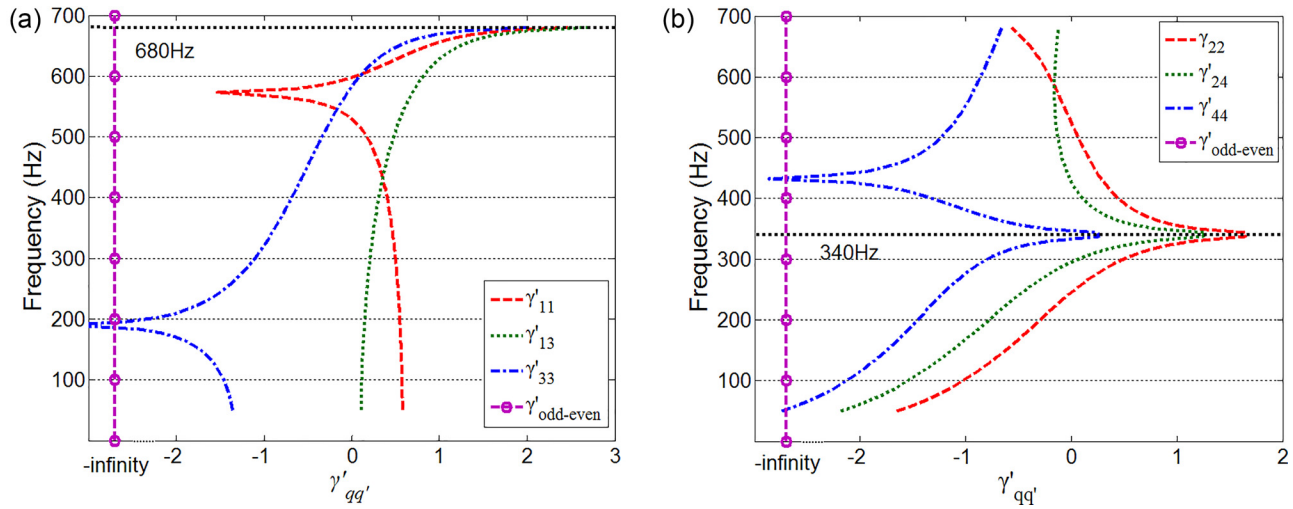

FIG. 10. (Color online) Variation of structural-acoustic coupling coefficients with excitation frequency: (a) $\gamma'_{odd\text{-}odd}$, (b) $\gamma'_{even\text{-}even}$.

0.05, 0.1, respectively. The two rows correspond to the dimensionless tension force $F^* = 0.6$ and 0.4, respectively. Optimal regions can be seen in these contour figures, with $S_1 = S_2 = 10^2$–10^4 N/m, and the ratio f_2/f_1 can reach 2.12 and 2.45 for $F^* = 0.6$ and 0.4, respectively, at Ma = 0. As the mean flow velocity increases, the optimal region is gradually deteriorated, especially for the lower tension $F^* = 0.4$. It indicates the benefit of maintaining a higher tension force in the presence of the mean flow.

Figure 12 shows the combined effect of the boundary conditions and the membrane tension force on f_2/f_1 at different Mach numbers. Here, the boundary restraint $S_1 = S_2$ is used to reduce the number of variables. Note that the ratio f_2/f_1 within the optimal window, $F^* = 0.4$–0.55 and $S_1 = S_2 = 10^2$–10^4 N/m, is likely reduce with increasing mean flow velocity, indicating a narrower sound attenuation stopband. For a higher tension force in the range of $F^* = 0.6$–0.8, however, the effect of the increase in the mean flow velocity has less influence on the transmission loss.

Let us now focus on two representative cases, marked as points A ($S_1 = S_2 = 6060$ N/m, $F^* = 0.7554$) and B ($S_1 = S_2 = 1650$ N/m, $F^* = 0.4174$) in two different regions in Fig. 12. Their corresponding transmission loss spectra are plotted in Fig. 13. Figure 13(a) illustrates that a higher tensile force helps maintain the sound attenuation performance during the increase of the mean flow. A comparison between Figs. 2(a) and 2(b) shows that the TL is more significantly affected by the mean flow velocities between the second and the third peaks, as compared to the region between the first and the second peaks. With the optimal parameter chosen within the optimal window, Fig. 13(b) shows that the third peak on the TL curve vanishes. Thus, the stopband

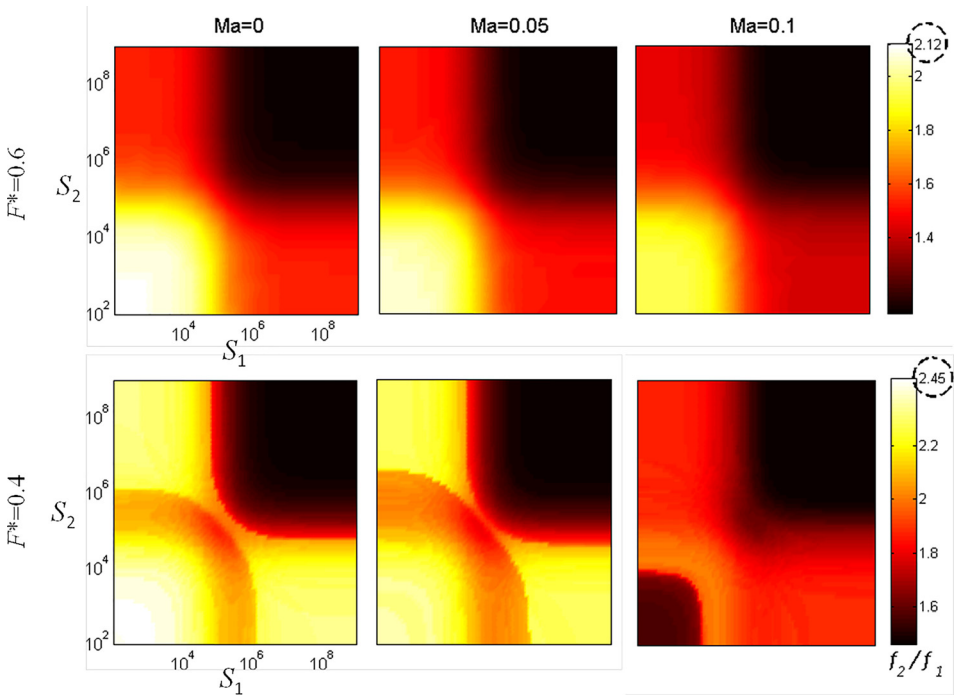

FIG. 11. (Color online) Influence of boundary restraining stiffness S_1 and S_2 on the stopband f_2/f_1 of current model with the values of Ma taken as 0, 0.05, 0.1, The first row: membrane tension $F^* = 0.6$. The second row: membrane tension $F^* = 0.4$.

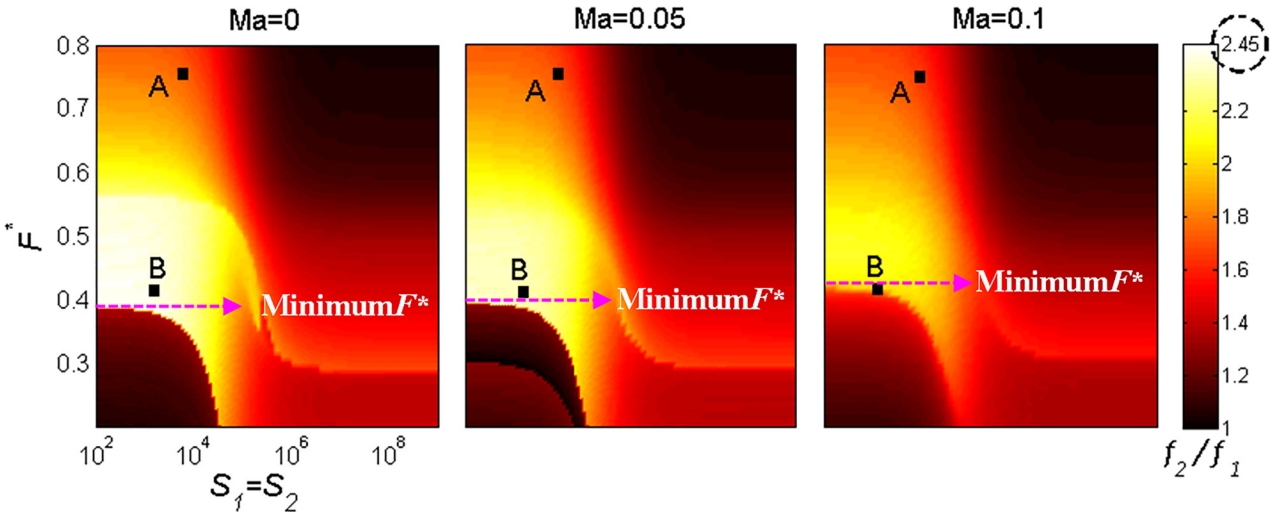

FIG. 12. (Color online) Influence of boundary restraint and tensile force on the ratio f_2/f_1 with Ma taken as 0, 0.05, 0.1.

characterized by the ratio f_2/f_1, can be significantly increased at lower Mach numbers with the proper tuning of the boundary restraints and the tensile force applied.

From the practical viewpoint, the selection of the membrane tension force is essential for achieving a good sound attenuation. As mentioned above, a higher tension force is helpful to maintain the sound attenuation performance in the presence of the mean flow. However, the side effect is the shifting of the stop-band towards the high frequency. To achieve the low-frequency noise reduction, a minimum tension force, referred to as the required minimum tension force, is crucial. Corresponding minimum F^* for different Mach numbers are marked in Fig. 12. Obviously, a higher tension force is needed to maintain a better sound attenuation when the mean flow speed increases. The variation of the required minimum tension force and that of the corresponding stopband ratio f_2/f_1 with respect to Mach numbers are plotted in Fig. 14, alongside the comparison with the case when F^* keeps a constant value of 0.38. Comparing the two curves in terms of the stopband ratio f_2/f_1, a remarkable difference can be observed when Ma exceeds 0.05. Obviously, the corresponding minimum F^* allows maintaining the sound attenuation. This figure provides guidance for the practical design of the system at different flow velocities.

IV. CONCLUSIONS

With the aim of fully understanding the vibro-acoustic coupling mechanism of a duct-mounted and cavity-backed membrane in the presence of grazing flow, an energy-based analytical formulation was proposed for the modelling of such a duct-membrane-cavity system. Boundary smoothed Fourier series and Rayleigh-Ritz procedure were employed to calculate the vibro-acoustic coupling response of such a system, in which the work done on membrane-fluid interface was chosen for the treatment of structural-acoustic interaction. Sound radiation into the duct from the membrane was characterized via a newly developed extension of the generalized Green's function theory in the presence of uniform mean flow.

The correctness and the effectiveness of the proposed model are validated through comparisons with results

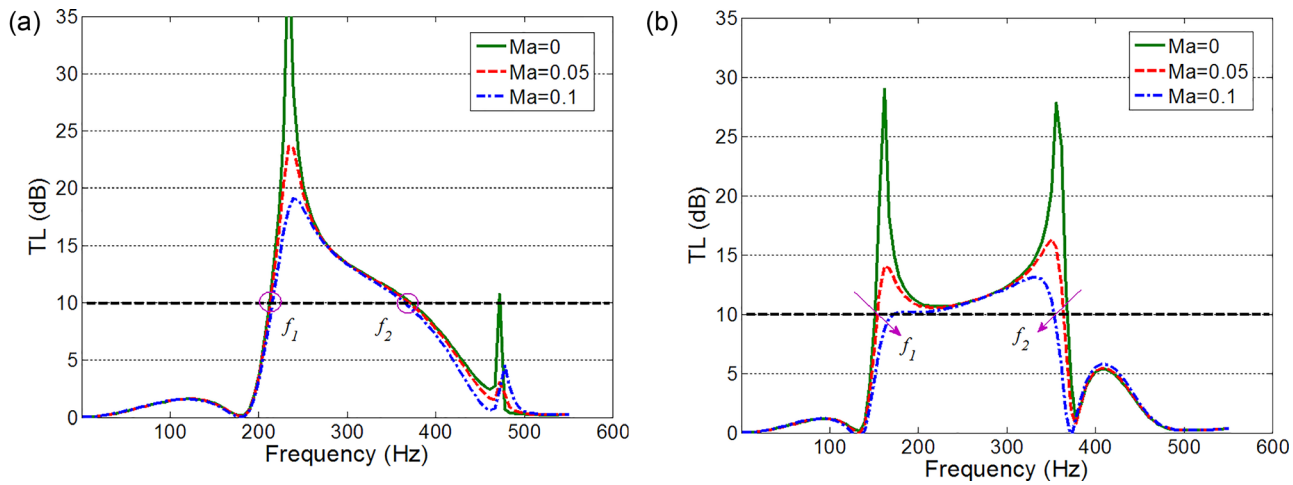

FIG. 13. (Color online) Transmission loss curves with combinations of boundary restraining stiffness and tensile force corresponding to selected points in Fig. 12: (a) point A, (b) point B.

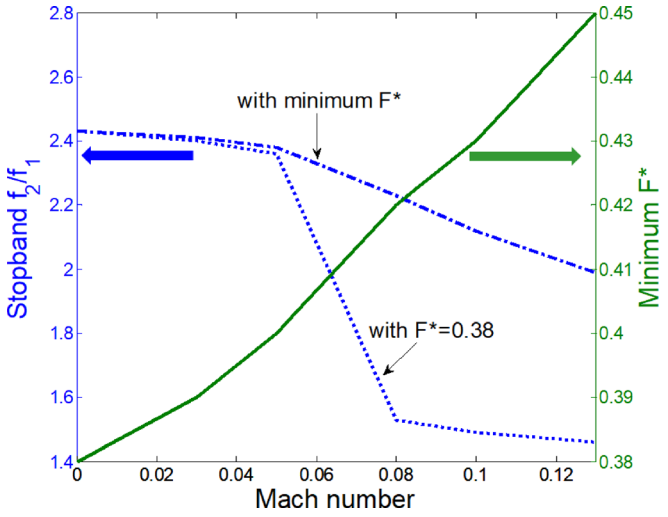

FIG. 14. (Color online) Variation of the stopband (left) and the required minimum F^* (right) with Mach number. Solid line: minimum tensile force; dash-dotted line: stopband with the required minimum F^*; dashed line: stopband with $F^* = 0.38$.

reported in the literature, showing consistent agreement in various cases. Based on the model, the vibro-acoustic coupling characteristics were investigated and discussed. Results show that the mean flow significantly affects the peak amplitude of the structural-dominant modal response, rather than their frequencies. Three cross-zones are observed on the kinetic energy spectrum of the membrane for various flow velocities within the frequency range considered in this paper. The first and the third cross-zones are dominated by membrane mode, and the second one by cavity mode. In the vicinity of these cross zones, the kinetic energy of the membrane is insensitive to the flow velocity, drastically different than other frequency regions. Furthermore, the membrane-duct and membrane-cavity structural-acoustic coupling coefficients were formulated to reveal and quantify the coupling mechanisms and strength. Results indicate that the general trend of membrane-duct coupling strengths of the odd-odd and even-even modes are insensitive to the Mach numbers, whilst those of the odd-even mode become more significant at higher Mach numbers. Finally, sound attenuation characteristics are also investigated by using the current model. Investigations on the combined effect of the boundary restraint and the tension force suggest that a proper adjustment of the boundary restraint with a higher tensile force is helpful to alleviate the adverse influence of the mean flow on the sound attenuation performance of such a duct-membrane-cavity system. It is believed that this work sheds light on the underlying physics and provides an efficient tool for guiding the practical design of such a duct-membrane-cavity system with the consideration of the mean flow.

ACKNOWLEDGMENTS

This work was supported by the Fok Ying Tung Education Foundation (Grant No. 161049) and Ph.D. Student Research and Innovation Fund of the Fundamental Research Funds for the Central Universities (Grant No. HEUGIP201806).

[1]F. J. Fahy, *Sound and Structural Vibration: Radiation, Transmission and Response* (Academic, New York, 1985), pp. 241–269.
[2]J. Pan and D. A. Bies, "The effect of fluid-structural coupling on sound waves in an enclosure—Theoretical part," J. Acoust. Soc. Am. **87**(2), 691–707 (1990).
[3]J. T. Du, W. L. Li, H. A. Xu, and Z. G. Liu, "Vibro-acoustic analysis of a rectangular cavity bounded by a flexible panel with elastically restrained edges," J. Acoust. Soc. Am. **131**, 2799–2810 (2012).
[4]P. E. Doak, "Excitation, transmission and radiation of sound from source distributions in hard-walled ducts of finite length (I): The effects of duct cross-section geometry and source distribution space-time pattern," J. Sound. Vib. **31**(1), 1–72 (1973).
[5]A. Cabelli, "The propagation of sound in a square duct with a non-rigid side wall," J. Sound. Vib. **103**, 379–394 (1985).
[6]A. Cabelli, "Application of the time dependent finite difference theory to the study of sound and vibration interactions in ducts," J. Sound. Vib. **103**, 13–23 (1985).
[7]A. Cummings, "The attenuation of sound in unlined ducts with flexible walls," J. Sound. Vib. **174**, 433–450 (1994).
[8]A. Cummings and R. J. Astley, "The effects of flanking transmission on sound attenuation in lined ducts," J. Sound. Vib. **179**, 617–646 (1995).
[9]A. Cummings, "Sound transmission through duct walls," J. Sound. Vib. **239**(4), 731–765 (2001).
[10]L. X. Huang, "Modal analysis of a drumlike silencer," J. Acoust. Soc. Am. **112**(5), 2014–2025 (2002).
[11]B. J. Tester, "The propagation and attenuation of sound in lined ducts containing uniform or 'plug' flow," J. Sound. Vib. **28**, 151–203 (1973).
[12]J. S. Alonso and R. A. Burdisso, "Green's functions for the acoustic field in lined ducts with uniform flow," AIAA J. **45**, 2677–2687 (2007).
[13]M. M. Sucheendran, D. J. Bodony, and P. H. Geubelle, "Coupled structural-acoustic response of a duct-mounted elastic plate with grazing flow," AIAA J. **52**(1), 178–194 (2014).
[14]G. Zhang, X. Wang, L. Li, X. Jing, and X. Sun, "Control of thermo-acoustic instability with a drum-like silencer," J. Sound. Vib. **406**, 253–276 (2017).
[15]Y. S. Choy, J. Huang, L. X. Huang, and Y. Zhou, "An experimental study of flow induced vibration on a tensioned membrane," J. Mech. Sci. Technol. **21**(9), 1359–1366 (2007).
[16]Y. S. Choy and L. X. Huang, "Effect off low on the drumlike silencer," J. Acoust. Soc. Am. **118**(5), 3077–3085 (2005).
[17]H. K. Fan, R. C. Leung, and G. C. Lam, "Numerical analysis of aeroacoustic-structural interaction of a flexible panel in uniform duct flow," J. Acoust. Soc. Am. **137**(6), 3115–3126 (2015).
[18]S. K. Tang, "Vortex sound in the presence of a low Mach number flow across a drum-like silencer," J. Acoust. Soc. Am. **129**(5), 2830–2840 (2011).
[19]Y. K. Chiang, Y. S. Choy, and S. K. Tang, "Vortex sound radiation in a flow duct with a dipole source and a flexible wall of finite length," J. Acoust. Soc. Am. **141**(3), 1999–2010 (2017).
[20]Y. Liu and J. T. Du, "Structural-acoustic interaction of a three-dimensional panel-cavity-duct system with non-uniform boundary restraints," J. Fluid. Struct. **79**, 94–114 (2018).
[21]Y. Liu and J. T. Du, "Coupling effect of boundary restraining stiffness and tension force on sound attenuation of a cavity-backed membrane duct silencer," Appl. Acoust. **117**, 150–159 (2017).
[22]M. Goldstein, "Unified approach to aerodynamic sound generation in the presence of sound boundaries," J. Acoust. Soc. Am. **56**, 497–509 (1974).
[23]S. W. Rienstra, "A classification of duct modes based on surface waves," Wave Motion. **37**, 119–135 (2003).
[24]K. U. Ingard, "Influence of fluid motion past a plane boundary on sound reflection, absorption, and transmission," J. Acoust. Soc. Am. **31**(7), 1035–1036 (1959).